Asthenospheric buoyancy and the origin of high-relief topography along the Cascadia forearc

M. Bodmer *, D.R. Toomey, J.J. Roering, L. Karlstrom

Department of Earth Sciences, University of Oregon, Eugene, OR 97403, USA

ABSTRACT

The forearc topography of the Cascadia subduction zone varies systematically along-strike, with high-relief in the north and south (the Olympic and Klamath ranges) separated by relatively low relief in its central region. This systematic topographic variability reflects the long-term pattern of uplift and erosion, however, the underlying cause of uplift and the mechanisms by which current topography is supported are unclear. Here, we synthesize results from seismic imaging, geodetic (decadal) and geomorphic (millennial) uplift rates, erosion rates, topographic analysis, and characteristics of the megathrust interface, with a mechanical model to infer that buoyancy in the subslab asthenosphere influences the development and longevity of Cascadia's forearc topography. The Cascadia margin can be divided into three broad segments, with the northern and southern segments characterized by rapid geodetic and geomorphic uplift rates, rapid erosion rates, high coseismic subsidence of great megathrust ruptures, shallower slab dip angles, and increased plate locking compared to the central segment. Tomographic images show low-velocity anomalies beneath the slab in the northern and southern segments, which are inferred to be regions of partial melt, resulting from localized upwellings, and regions of positive mantle buoyancy. Modeling suggests that these buoyant regions can locally increase the total shear force at the megathrust by either shallowing the slab dip — thereby increasing the area of the seismogenic zone — or increasing mechanical plate coupling along the megathrust, by increasing normal stress and/or the effective coefficient of friction. We propose that: 1) sub-slab buoyancy influences topographic development by modulating along-strike patterns of strain within the over-riding plate during the seismic cycle, 2) Permanent development of surface topography occurs due to unrecovered strain over thousands of seismic cycles, and 3) variations in Cascadia's forearc topography are laterally supported by changes in the total shear force at the megathrust interface. Using independent estimates for slab dip and plate locking, we predict the first-order variations in Cascadia forearc topography, with local maxima in the north and south as observed. Given our results, variations in subslab buoyancy may be critical to explaining forearc topography in other subduction systems.

© 2019 Elsevier B.V. All rights reserved.

1. Introduction

The mechanics of convergent margins influence the forces that generate and support forearc topography (e.g. Cattin et al., 1997). Forearc morphology varies both globally and within subduction zones (Bassett and Watts, 2015) and many convergent margins exhibit along-strike variations in plate locking and seismicity (Ando, 1975; Kopp, 2013). Though pressure and temperature conditions control the first-order behavior downdip (Hyndman and Wang, 1993), most studies investigating behavioral segmentation along-strike focus on lateral variations in properties of the thrust inter-

face or adjacent crust (Brudzinski and Allen, 2007; Cloos, 1992; Delph et al., 2018; Janiszewski et al., 2019; Littel et al., 2018). Recent findings, however, suggest that dynamics of oceanic asthenosphere beneath the down-going plate contribute to along-strike segmentation (Bodmer et al., 2018). Here, we explore the relationship between upper mantle processes, megathrust dynamics, and the evolution of the forearc landscape.

We focus on the Cascadia subduction zone, exploiting the wealth of observations spanning large spatial (upper mantle to surface) and temporal (decades to millions of years) scales. Two regions of high-relief topography are present in the forearc (the Olympic and the Klamath ranges; Fig. 1), separated by the relatively low-relief Oregon Coast Range. Similarly, there is evidence from multiple observations for segmentation of megathrust behavior, specifically from historic large earthquakes, episodic tremor
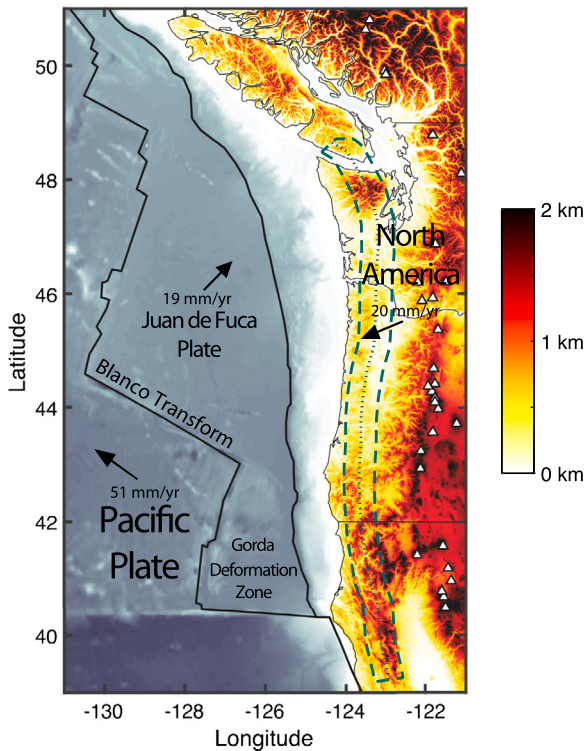
Fig. 1. Topographic map of the Cascadia subduction zone. Regions of high forearc topography are observed in northern and southern Cascadia, the Olympic and Klamath ranges, respectively. Arrows represent absolute plate motions in a hotspot reference frame (DeMetts et al., 2010). White triangles represent current and historic volcanism. Green lines denote the swath used to plot several of the datasets in subsequent figures. (For interpretation of the colors in the figure(s), the reader is referred to the web version of this article.)

and slip, inferred plate locking, and seismicity (Brudzinski and Allen, 2007; Goldfinger et al., 2012; Li et al., 2018; McCrory et al., 2012; Schmalzle et al., 2014; Wells et al., 2017). Previous work suggested that differences in incoming plate age drive topographic variation (Kelsey et al., 1994), however we show that more recent observations are inconsistent with this interpretation.

In this paper, we synthesize along-strike characteristics of the Cascadia margin in order to address two questions: 1) What conditions give rise to long-term uplift and development of differential topography in the forearc? 2) What are the mechanisms that support current forearc topography? We infer that buoyant asthenosphere beneath the subducting slab (Bodmer et al., 2018) influences both of these processes by modulating megathrust properties (slab morphology and/or mechanical coupling of the plates) and thus contributes to the first-order response of the overlying landscape.

2. Tectonic setting

The Cascadia subduction zone (CSZ) is where the Juan de Fuca (JdF) plate converges with North America at a rate of ~40 mm/yr (DeMets et al., 2010) (Fig. 1). The CSZ rupture cycle is estimated to be 300–500 yr, with the last great earthquake (M9.0) in 1700 AD (Goldfinger et al., 2012). The offshore plate system includes the JdF and two smaller fragmenting regions, the Explorer plate and Gorda deformation zone (GDZ), to the north and south respectively. The age of JdF crust entering the subduction zone is young (<10 Ma). Beneath the forearc, ages vary gradually along-strike, despite the presence of the Blanco Fracture Zone (BFZ) offshore. This is because the BFZ is a recent feature (~4 Ma) resulting from plate reorganization in the last ~8 Ma (Riddihough, 1984; Wilson, 2002;

Fig. S1). The convergent margin is short, ~1000 km in length, yet multiple studies indicate that structure and behavior vary along strike. We define three main segments (northern, central, southern; Fig. 1) from observations of megathrust behavior (see Sec. 3) in order to locate and compare key features.

The Olympic mountain range is a forearc high (peaks >2 km above sea level) located in northwest Washington, in the northern segment of Cascadia (Fig. 1). Glaciation in the Olympics is present currently at altitudes of 1.7 km (Fountain et al., 2017) and average relief (within a 2.5 km radius) reaches ~1.2 km (Fig. S2). This region is comprised of Miocene marine sedimentary rocks and is a subaerial subset of a larger regional subduction complex (Tabor and Cady, 1978). The mountainous core is surrounded by a horseshoe shaped belt of Eocene oceanic basalt (Tabor and Cady, 1978). These basalts are a part of the large igneous province Siletzia, which extends south into central Oregon and was accreted at ~50 Ma (Wells et al., 2014). The Olympics are located inboard of a change in margin strike and have a small lateral dimension (~100 km). High elevations are also observed just north in the Vancouver portion of the Wrangellia terrain. Uplift of the Olympics started ~18 Ma and topography is thought to be steady state, implying average rates of uplift and erosion that are nearly equivalent over the region (Brandon et al., 1998; Brandon and Calderwood, 1990; Pazzaglia and Brandon, 2001). Though the steady state assumption is widely used in the Cascadia forearc, increases in sediment flux due to Quaternary glaciation have been inferred to influence subduction mechanics (Adam et al., 2004; Booth-Rea et al., 2008) and may impact orogenesis.

The Klamath range is a forearc high (peaks >2 km above sea level) located in northern California and southern Oregon, in the southern segment of Cascadia (Fig. 1). Glaciation in the Klamaths is currently present in a small area (<2 km^2) located in the Trinity Alps (Fountain et al., 2017) and average relief (within a 2.5 km radius) reaches ~1 km (Fig. S2). The range is comprised of various oceanic terranes accreted during the Paleozoic through to Jurassic time (Snoke and Barnes, 2006). The Klamaths are located east of the GDZ and north of the Mendocino triple junction, the transition from transform motion along the San Andreas fault system to convergence at the CSZ. Uplift of the Klamath range is thought to have initiated most recently in the last ~3 Ma, as inferred from the presence of a well-developed erosional surface in the western range, the Klamath peneplane, which formed ~5 Ma (Aalto, 2006; Diller, 1902; Mortimer and Coleman, 1985). Evidence of earlier (Oligocene-Eocene) topographic development associated with the accretion of Siletzia and extension of the La Grange fault has been inferred for the southeasternmost Klamaths (Batt et al., 2010; Piotraschke et al., 2015).

Separating the Olympics and Klamath ranges are the relatively low-relief Coast Ranges, located in the central segment (Fig. 1). The Coast Ranges exhibit average topography less than 0.5 km above sea level (peaks reaching 1 km) and are unglaciated. The Coast Ranges are comprised of Eocene sedimentary deposits overlaying the accreted Siletzia terrane (Heller and Ryberg, 1983). Uplift of the Coast ranges is thought to have occurred since 15–16 Ma (McNeill et al., 2000) and is in topographic steady state with erosion (Roering et al., 2007).

3. Results from previous studies

To address the development and mechanical support of forearc topography in Cascadia, we first synthesize observations and inferences from previous work. These studies span several spatial and temporal scales, addressing: erosion and vertical uplift of the forearc (Sec. 3.1); role of isostasy in supporting forearc topography (Sec. 3.2); structure and dynamics of the upper mantle beneath the subducting slab (Sec. 3.3); properties of the subducting plate
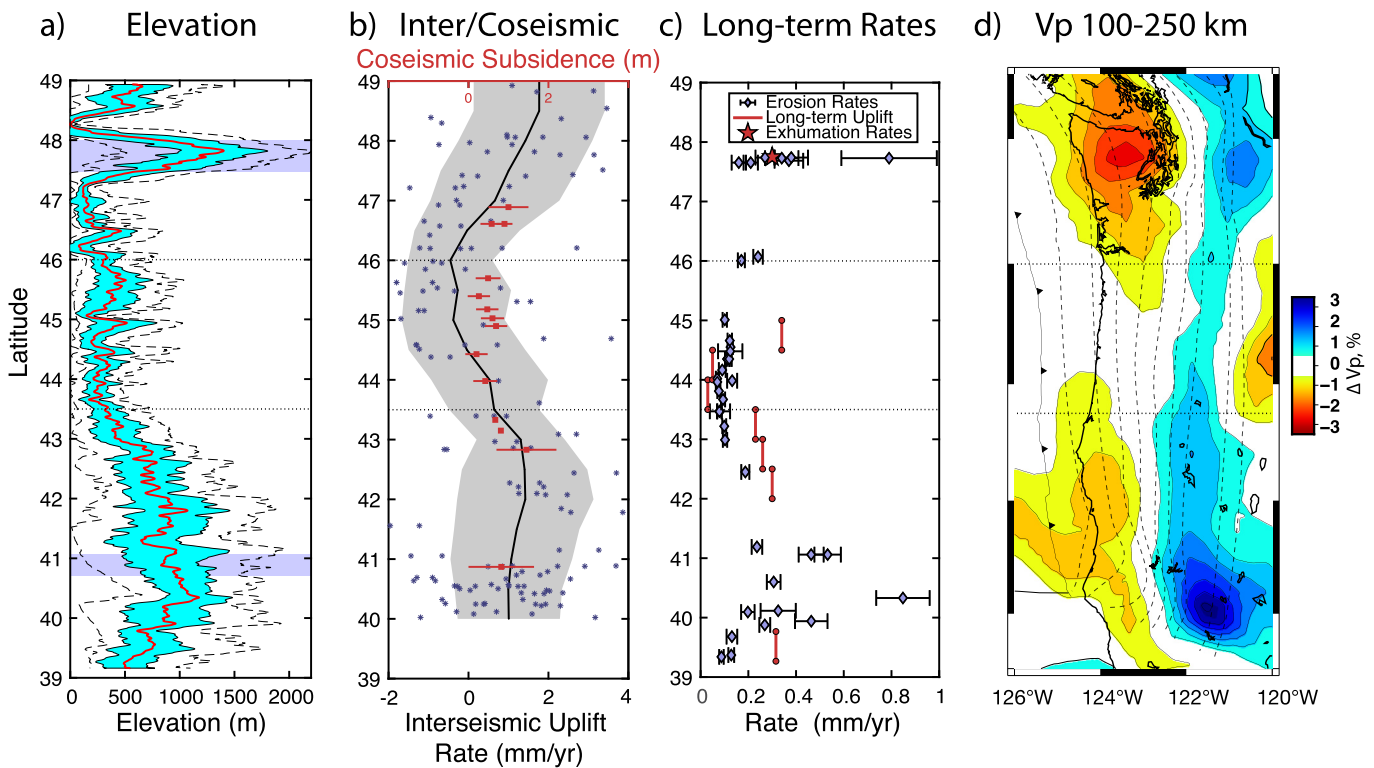
Fig. 2. Along-strike variations in the landscape evolution of the Cascadia forearc. Horizontal dotted lines at 46N and 43.5N represent inferred segment boundaries separating northern, central, and southern segments. See Sec. 3.1 for sources. a) Forearc topography within the ~100 km wide swath (Fig. 1). Red line represents mean elevation, dashed lines represent minimum and maximum elevations, and blue area represents one standard deviation. Purple bars represent latitudes where Pleistocene glaciation is observed in the forearc. b) Interseismic uplift rates and coseismic subsidence. Blue dots represent individual GPS vertical velocities within and to the west of the swath, black line represents the average vertical velocity, and the shaded region represents one standard deviation. Red symbols represent coseismic subsidence during the 1700 event. Note the two datasets are plotted on different scales. c) Long term uplift rates and erosion rates. Red lines represent averaged long-term uplift rates from shorecut platforms. The red star represents exhumation rate estimate from the Olympics. Purple diamonds represent erosion rates from cosmogenic radionuclide concentrations. d) Tomographic image of relative P-wave velocities averaged between 100–250 km depth. This depth represents the subslab region. Dashed lines represent depth contours to top of slab (10 km increments).

interface (Sec. 3.4); and mechanical modeling of the forearc relating plate interface forces to forearc characteristics (Sec. 3.5).

3.1. Topographic evolution of the Cascadia forearc

Vertical motion of the Cascadia forearc varies along-strike, with the spatial patterns from multiple observations reflecting the segmentation boundaries defined by megathrust behavior (Fig. 2). These observations broadly fall into two categories: short-term processes on the scale of an individual seismic cycle and long-term processes occurring over many seismic cycles, up to millions of years. Observations across scales suggest increased uplift rates in the northern and southern segments.

Topographic highs are observed in the northern and southern segments of the Cascadia forearc corresponding to the Olympic and Klamath ranges respectively. The topographic profile, Fig. 2a, is derived from 30 m resolution DEM's within a ~100 km wide swath (see Fig. 1). Local maximum elevations in the northern and southern segments are 2.2 km and 1.9 km with mean elevations of roughly 1.4 km and 1.0 km, respectively. Comparatively, central Cascadia's coast range only reaches a maximum elevation of 1.0 km with a mean elevation of 0.4 km. The forearc highs differ in spatial dimensions, with the Olympics being a narrow feature (~100 km width) and the Klamath's more laterally expansive (~300 km width). These topographic patterns reflect the net result of the competition between vertical uplift and denudation processes and it is unlikely that they are the result of rock type variation (Kelsey et al., 1994). Although our analysis doesn't require it, long-term uplift and erosion data support an approximate

balance between uplift and erosion and steady topographic form (Willett and Brandon, 2002).

Measurements of short-term vertical motion are larger in the northern and southern segments, co-located with regions of high topography (Fig. 2b). Observations come from interseismic GPS measurements and coseismic subsidence estimates, both of which capture deformation during a single seismic cycle. GPS measurements from Plate Boundary Observatory (PBO) stations display average uplift rates of 1–2 mm/yr in northern and southern Cascadia, with maximums reaching 5 mm/yr (Fig. 2b; Schmalzle et al., 2014). Conversely, average vertical rates in central Cascadia are indistinguishable from zero. The variance of GPS derived velocities is large; however, the pattern of observations is corroborated by tide gauge and leveling data (Burgette et al., 2009). Estimates of coseismic subsidence during the 1700 Cascadia megathrust rupture, derived from tidal microfossil studies (Wang et al., 2013), show a decrease in subsidence within the central segment (0.5–1 m compared to the north/south segments; Fig. 2b). Wang et al. (2013) infer a heterogeneous rupture pattern with four high slip patches, but in general, coseismic subsidence is observed to be lower in central Cascadia for several previous ruptures (Leonard et al., 2010).

Estimates of long-term vertical motion, averaging over many seismic cycles, display similar patterns with increased uplift and erosion rates in the northern and southern segments (Fig. 2c). Long-term uplift rates, averaged from shoreline platform analysis estimates (Balco et al., 2013; Kelsey et al., 1994; 1996), and exhumation rates, from apatite fission track analysis (Brandon et al., 1998), show increased rates north and south compared to the central segment (Fig. 2c). Compiled erosion rate estimates, derived
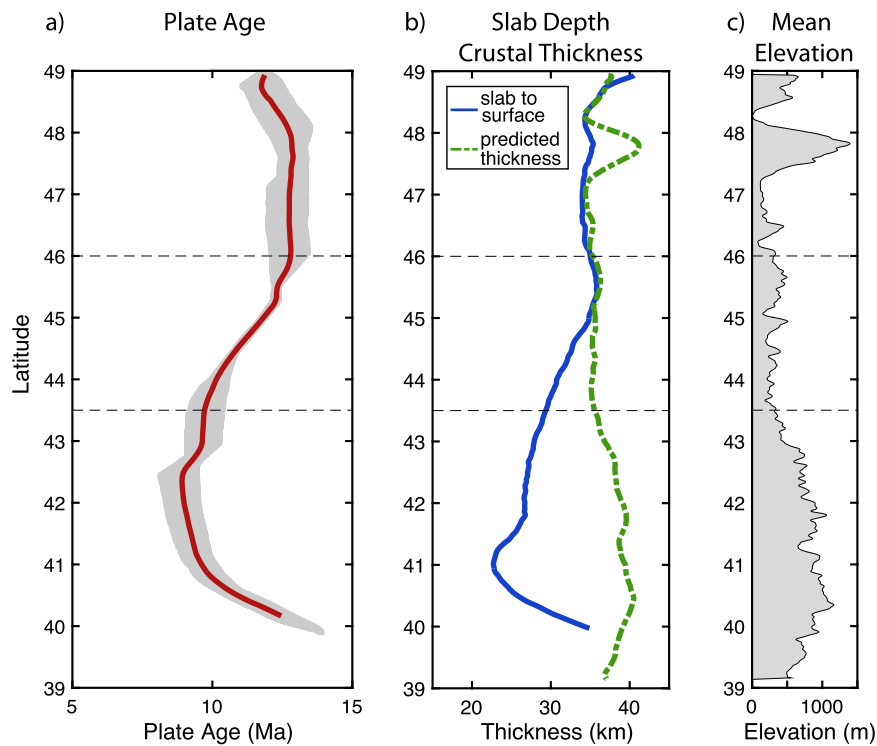
Fig. 3. a) Plate age variations beneath the forearc swath (see Fig. S1). Red line represents the average and the gray area the total range of the data. Calculated from Wilson (2002). b) Comparison of slab depth to predicted crustal thickness. Blue line is the average depth to slab beneath the swath. Green line is the predicted crustal thickness from the observed topography assuming full isostatic compensation. Slab depth from McCrory et al. (2012). c) Mean elevation within the forearc swath. Horizontal lines at 46N and 43.5N represent inferred segment boundaries.

from cosmogenic radionuclide data, suggest rates approaching 1 mm/yr in northern and southern Cascadia, whereas central Cascadia rates are lower, ∼0.2 mm/yr (Fig. 2c; Balco et al., 2013; Bierman et al., 2001; Ferrier et al., 2005; Fuller et al., 2009; Livermore, 2001; Marshall et al., 2017; Penserini et al., 2017; Roering et al., 2015). Cosmogenic radionuclide erosion rates estimates are ideal because they are robust against anthropogenic change. Consistent with the notion of steady state topography, the magnitudes of long-term uplift rates and erosion rates are broadly in agreement. However, long-term uplift and erosion rates are approximately an order of magnitude lower than the short-term, interseismic uplift rates (Fig. 2b–c; Penserini et al., 2017), which reflects a snapshot of elastic strain accumulation in the earthquake deformation cycle, similar to other subduction zones (Ramírez-Herrera et al., 2018).

3.2. Isostacy of the subducting plate and overriding crust

Here we estimate the isostatic contributions of the subducting slab and the overriding crust to forearc elevation; subslab contributions are addressed in Sec. 3.3. We show that contributions due to oceanic plate age differences are negligible and our results imply insufficient accommodation space above the subducting slab for the crustal thickness variations required to support topography.

Kelsey et al. (1994) suggested that isostatic adjustments due to along-strike changes in plate age support forearc topography, with high-standing relief underlain by younger oceanic crust. Their study assumed that the BFZ corresponds with a >10 My age offset in oceanic lithosphere beneath the forearc that migrates northward. Reorganization of the JdF plate system and subsequent development of the BFZ, however, did not begin until ∼8 Ma and ∼4 Ma, respectively (Riddihough, 1984; Fig. S1). A more recent plate reconstruction by Wilson (2002) shows that plate age beneath the forearc differs by at most 4 My and that age does not correlate with the forearc relief pattern (Fig. 3a). Further, using a

half-space cooling model and plate ages from Wilson (2002), we calculate ∼200 m of isostatic elevation variation, an order of magnitude lower than the observed topography (Fig. 3c), which is less than half the previous estimate (Kelsey et al., 1994). Several offshore studies indicate that the JdF plate is not consistent with the half space cooling model (Bell et al., 2016; Byrnes et al., 2017; Eilon and Abers, 2017), with estimates of lithospheric thickness variations on the order of 10–15 km (Rychert et al., 2018) corresponding to ∼450 m of isostatic elevation variation. This amplitude is still far less than the observed topography and, further, the spatial patterns of the two datasets along-strike do not appear well correlated.

Using the depth to the slab interface as an absolute bound on crustal thickness, we find that there is insufficient space for the thickness of continental crust needed to isostatically support topography. Fig. 3b shows an estimate of the maximum possible thickness of the crust beneath the forearc, assuming that continental crust extends down to the slab interface of McCrory et al. (2012). Notably, despite the high standing topography in southern Cascadia, the forearc crust is relatively thin in this region. Global studies indicate an average elevation of 800 m and crustal thickness of 38 km (Amante and Eakins, 2009; Christensen and Mooney, 1995), which we use as an isostatic reference. Assuming average crustal and mantle densities of 2.8 $\frac{g}{m^3}$ and 3.3 $\frac{g}{m^3}$, respectively, crustal thicknesses of 43 km and 40 km are required to isostatically support the mean topography in northern and southern Cascadia. This is 5–15 km thicker than the local depth to the slab interface (Fig. 3b; McCrory et al., 2012) and crustal thickness estimates for the region (Gilbert, 2012; Shen et al., 2013). In contrast, crustal thickness in central Cascadia is more consistent with isostatic support (Fig. 3b), though other forces likely contribute to topographic development and support.

We can also estimate along-strike changes in elevation due to crustal thickness variations and find that predicted patterns do
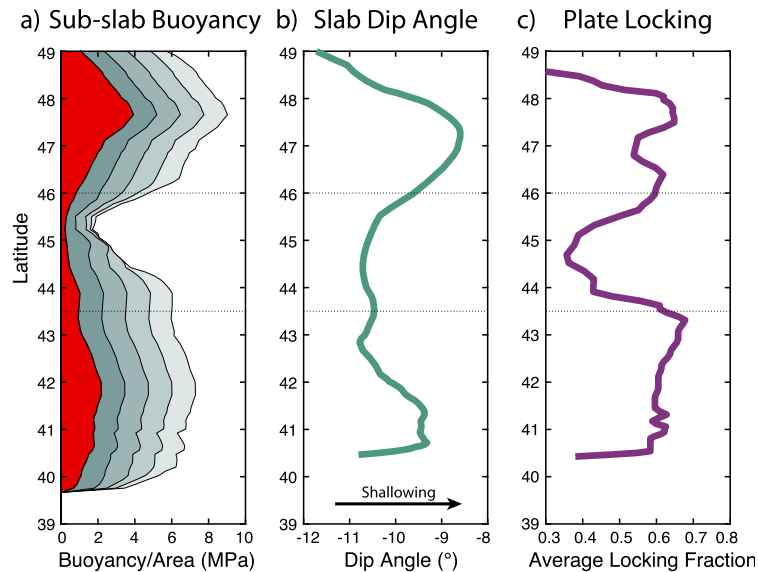
Fig. 4. Along-strike variations in the subslab mantle, slab geometry, and estimated coupling along the megathrust interface. Horizontal dashes represent inferred segment boundaries. a) Subslab buoyancy estimate inferred from the seismic tomography (Fig. 3d). Red area represents buoyancy/area estimate if low-velocities are due solely to partial melt. Grey regions represent buoyancy/area estimates if temperature is allowed to contribute (temperature capped in increments of 10 K). From Bodmer et al. (2018). b) Average slab dip angle in the shallow portion of the megathrust interface. The maximum slab depth considered is 30 km. Calculated from McCrory et al. (2012). c) Average plate locking. Average is taken in a 50 km wide swath around the maximum value for a given latitude using the Gaussian locking model from Schmalzle et al. (2014).

not correlate with the observed topography (Fig. S3). Two crustal thickness estimates are taken from seismic studies (10–15 km of variation along-strike; Gilbert, 2012; Shen et al., 2013) and another from the inferred surface-to-slab maximum (McCrory et al., 2012). These results show up to 2 km of topographic variation, however the along-strike patterns are inconsistent with the observed topography. Lastly, we can estimate the along-strike changes in crustal density required to support the observed topography (Fig. S3). We find average crustal densities of 2.2–2.6 $\frac{g}{m^3}$ in the north and 2.3–2.5 $\frac{g}{m^3}$ in the south would be required. Using the Nafe-Drake curve (Brocher, 2005), this corresponds to average crustal Vp values (ranging from 3.0–5.3 km/s) that lie more than 2σ below the global average (6.45 ± 0.23 km/s; Christensen and Mooney, 1995), and below average crustal values in Cascadia (~5 km/s; Parsons et al., 2005; Trehu et al., 1994) except at their maximum limit. Moreover, the required variation of average density along-strike would result in average crustal velocity variations of ~1.7 km/s, roughly equivalent to the entire range of observed crustal velocities globally (Christensen and Mooney, 1995). We conclude from these comparisons that forearc topography in Cascadia is not supported isostatically by either the crust or buoyancy variations due to age differences of the subducting plate.

3.3. Subslab buoyancy

A recent seismic study of the CSZ identifies two localized low-velocity anomalies beneath the subducting slab in northern and southern Cascadia (Fig. 2d; Bodmer et al., 2018) that are co-located with regions of high topography, increased uplift rates, increased erosion rates, and larger coseismic subsidence (Sec. 3.1; Fig. 2a–c). In northern Cascadia, the seismic anomaly ($\Delta V_P \approx -3\%$) is attributed to upwelling and decompression melting of relatively warm mantle entrained (Bodmer et al., 2015) from the nearby Cobb hotspot. In southern Cascadia the seismic anomaly ($\Delta V_P \approx -1.5\%$) is attributed to upwelling and decompression melting of asthenosphere from beneath the subducting slab, driven by rapid

northwest motion of the Pacific plate with respect to a relatively stagnant GDZ.

Due to presence of partial melt — and possibly a thermal anomaly in northern Cascadia — Bodmer et al. (2018) infer that these mantle upwellings generate positive buoyancy beneath the slab. If the subslab low-density anomalies present between 100 and 250 km depth are isostatically compensated by surface uplift, they would generate an along-strike pattern comparable to observed forearc relief, however, the magnitude of uplift (~200 m) would be an order of magnitude less than observed (Fig. S3). A positive buoyancy force, however, would push upward on the base of the subducting plate with an average increase in force per unit area of 2–8 MPa in northern and southern Cascadia (Bodmer et al., 2018; Fig. 4a). These forces could deflect the subducting slab upward, resulting in regional scale variations in slab morphology and dip. Because density contrasts between the upwardly buoyant subslab asthenosphere and the overlying slab are small, the vertical deflection of the slab will be greater than the magnitude of surface uplift. Additionally, this buoyancy force could increase stress on the megathrust interface. In the next section (Sec. 3.4) we summarize observations at the slab interface consistent with these ideas.

3.4. Along-strike variations of the slab interface

Geometry of the slab, as well as the coupling between plates, can influence both the stress accumulated and released during the seismic cycle (Bletery et al., 2016; Schmalzle et al., 2014) and the stresses that support the forearc wedge (Dahlen, 1990; Wang and He, 1999). Slab geometry and mechanical plate coupling are also properties that may be influenced by subslab buoyancy forces (Betts et al., 2012; Bodmer et al., 2018).

The morphology of the JdF slab interface varies both along-strike and down-dip (Bostock et al., 2019; McCrory et al., 2012; Fig. 2d, 4c). Depth to interface estimates have been made for Cascadia down to 100 km depth, using earthquake locations and regional seismic studies (McCrory et al., 2012). First order features
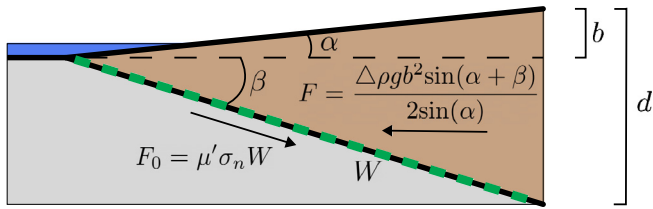
F: Gravitational stretching force
F₀: Total shear force
Δρ: density difference between crust and structure left of the wedge
g: acceleration due to gravity
μ′: Effective coefficient of friction
α: Topographic relief angle
β: Slab dip angle
b: Forearc topography
W: Width of plate coupling
d: Depth limit of coupling

Fig. 5. Schematic model illustrating the force balance between gravitational forces promoting the stretching/collapse of the forearc wedge and the resistive shear forces along the megathrust interface. For Cascadia $F \approx F_0$.

include a broad flattening of the subducting slab in the northern segment, where the strike of subduction rotates, and evidence of a slab buckle in the southern segment, near the Mendocino triple junction. There is also evidence for along-strike changes in the average dip angle within the shallow (<30 km depth) and potentially locked portion of the interface (Fig. 4b). Average interface dip angles are shallower in the northern and southern segments, compared to the central segment, varying by 2.5° and 1.5°, respectively.

The degree of interface plate locking (the kinematic description of slip at a given moment in the seismic cycle), inferred from onshore geodetic observations (Li et al., 2018; Schmalzle et al., 2014), also display along-strike variation. Fig. 4c estimates the average plate locking along-strike (for a 50 km wide E-W band centered on the local locking maximum) using the Gaussian model from Schmalzle et al. (2014). The northern and southern segments have a ∼25% increase in locking compared to central Cascadia. These geodetic models are non-unique, in part because of poor constraints offshore, but decreased locking in central Cascadia appears to be a robust feature. Current plate locking (kinematic) does not have to reflect the long-term state of mechanical plate coupling (stress and frictional properties) (Wang and Dixon, 2004), however, in Cascadia the pattern of locking is consistent with patterns of long-term uplift rates and forearc topography.

Both shallower interface dip angles and increased plate locking correlate with regions of increased subslab buoyancy (Fig. 4a) and increased uplift in the forearc (Fig. 2a–c). In Sec. 3.5 we explore how these variations can influence forces along the megathrust interface and in the forearc.

3.5. Mechanics of the forearc

The long-term mechanics of the subduction zone forearc can be expressed in terms of the total shear force along the megathrust interface and opposing gravitational forces at the interface, which promote stretching and collapse of the forearc (Fig. 5; Dahlen, 1990; Wang and He, 1999). Here, we present a quasi-static 2D along-dip model of the forearc which we will use to relate subslab buoyancy to topography (Fig. 5), assuming steady state topography so that erosion does not influence the force balance as has been proposed for connections between glaciations and deep melt generation in volcanic regions (e.g., Huybers and Langmuir, 2009).

Following Wang and He (1999), we define the trenchward stretching force, F, and the total shear force along the megathrust interface, F_0. The stretching force (F) arises due to topographic relief in the forearc being laterally unconstrained, resulting in devi-

atoric horizontal tension in the lower part of the plate. It is defined as:

$$F = \frac{\Delta \rho g b^2 \sin(\alpha + \beta)}{2 \sin(\alpha)} \quad (1)$$

where $\Delta \rho$ is the average density contrast between the forearc and material left of the wedge (approximated here as $\Delta \rho = 2 \frac{g}{cm^3}$), g is acceleration due to gravity, b is the height above the incoming or undeformed oceanic plate, α is the angle of the topographic relief with respect to the incoming oceanic plate, and β is the interface dip angle (Fig. 5).

The total shear force along the megathrust interface is due to frictional coupling of the plates. It is defined as:

$$F_0 = \mu' \sigma_n W \approx \frac{1}{2} \mu' W d \rho g \quad (2)$$

where μ' is the effective coefficient of friction, ρ is the density of the forearc wedge, W is the downdip width of the coupled region, and we assume the plates become uncoupled at critical depth, d, perhaps dependent on the thermal structure (Hyndman and Wang, 1995). Mechanical plate coupling is defined as the level of long-term stress on the interface using a static friction law $\tau = \mu' \sigma_n$ (Wang, 2000; Wang and Dixon, 2004), where τ is the shear stress and σ_n is the normal stress. The effective coefficient of friction μ' contains contributions from the static coefficient of friction, pore pressure effects from fluids, and any other conditions that may influence frictional properties. This describes a long-term interaction along the interface as opposed to the short-term kinematic plate locking condition, the latter of which may change between or during seismic cycles. The width of the coupled region can be defined as a function of the coupling depth limit d and interface dip β, such that $W = \frac{d}{\sin(\alpha) + \sin(\beta)}$. Thus, a decrease in interface dip increases the coupled width and the total shear force can be rewritten as,

$$F_0 = \frac{\mu' \sigma_n d}{(\sin(\alpha) + \sin(\beta))} \quad (3)$$

here, the magnitude of F_0 depends on both the interface dip angle (modulating the coupled width, W) and mechanical plate coupling ($\mu' \sigma_n$). The total shear force at the megathrust interface increases due to shallowing the interface dip angle or increasing mechanical plate coupling (Fig. S5).

We can link forearc topography to the total shear force by relating equations (1) and (3). For Cascadia $F \approx F_0$ (Wang and He, 1999). Thus:

$$\frac{\Delta \rho g b^2 \sin(\alpha + \beta)}{2 \sin(\alpha)} \approx F_0 = \frac{\mu' \sigma_n d}{(\sin(\alpha) + \sin(\beta))} \quad (4)$$

This describes a forearc dynamically supported by the long-term shear forces at the interface. Using reference values of $\alpha = 1.5°$, $\beta = 11.5°$ (average dip angle in central Cascadia), and $b = 4$ km (measured from the top of the oceanic crust; appropriate for Cascadia after ignoring the ∼1 km thick sediment layer), we estimate a 25% increase in the resistive shear force is needed to support a 1 km increase in forearc topography (Fig. S5). Using reference value $\mu' = 0.03$ (Wang and He, 1999), we estimate that a 1 km increase in forearc topography requires either a 2° shallowing of the slab dip or a 33% increase in the mechanical plate coupling $\mu' \sigma_n$ (Fig. S5).

4. Discussion

We propose that buoyant anomalies in the subslab region locally increase the total shear force along the megathrust through

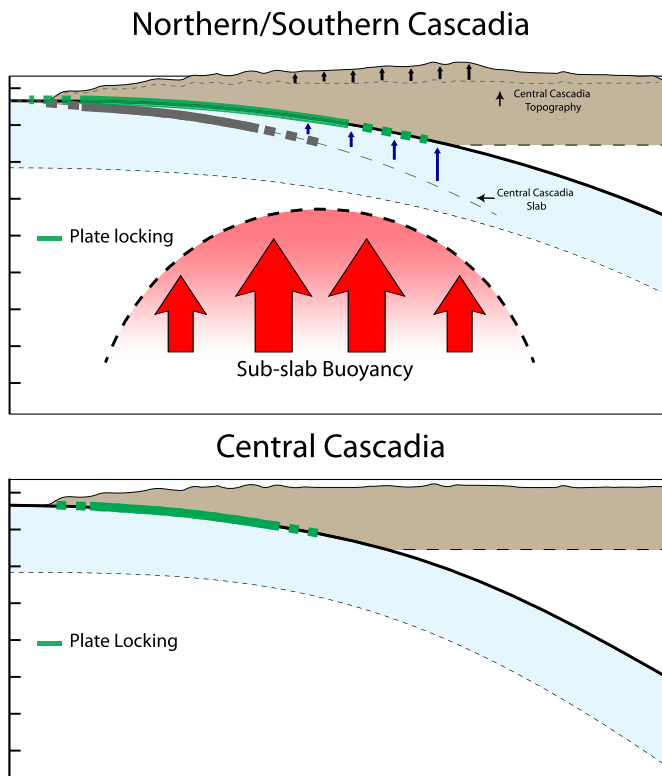## Northern/Southern Cascadia

Central Cascadia

Fig. 6. Conceptual model for the Cascadia subduction zone. In northern and southern Cascadia subslab buoyancy influences the overlaying megathrust by changing the slab morphology (shallowing the dip) and increasing the degree of mechanical plate coupling. This leads to preferential growth of topography in these regions and provides support for the high standing topography that is present. In central Cascadia, where subslab buoyancy is absent, slab dips are steeper and coupling is reduced leading to reduced topographic development and supported topography.

some combination of decreased average dip angle of the shallow subduction interface and increased mechanical plate coupling (Fig. 6). These factors can influence short-term processes such as where interseismic uplift and plate locking occur. In the long-term, if interseismic uplift is consistently related to the long-term uplift pattern, then total shear force variations affect where excess topography is most likely to develop. Thus, subslab properties influence along-strike variations in forearc vertical motion through time. Further, we suggest that along-strike changes in the total shear force acting on the thrust interface support the variable topography in the forearc.

4.1. Influence of subslab buoyancy on the megathrust interface

Along-strike variations in subslab buoyancy could impact slab morphology, locally shallowing the slab in regions overlaying buoyant anomalies. This notion is similar to the morphology of subducting slabs being dependent on their density structure, with more buoyant (younger) slabs tending towards flat subduction (Royden and Husson, 2009). The age of the JdF slab varies by <4 Ma beneath the forearc (Wilson, 2002; Fig. 3), thus the expected density variation of the slab is low. However, the young age of the slab (~10 Ma), and corresponding low elastic thickness ($T_e \approx 8.5$ km with a flexural wavelength ≈ 1 km), make it more susceptible to morphologic changes due to insignificant flexural response. Geodynamic models have shown that introducing buoyant material into a subduction zone impacts the dynamics, locally shallowing slab dip angles, advancing the subducting trench, and modifying the strike of the subduction zone (Betts et al., 2012). Observations of decreased slab dip in northern and southern Cascadia (Fig. 4) are consistent with an upward directed force acting on the slab

from below, working in opposition to forces associated with crustal loading and slab pull.

We postulate that excess subslab buoyancy may also change the state of stress at the megathrust interface, locally increasing mechanical plate coupling above buoyant regions. Mechanical plate coupling (stress and frictional properties) can be increased in two ways, either by increasing the normal stress σ_n or increasing the effective coefficient of static friction μ'. Increases in normal stress could arise if the flexural rigidity of the overlaying crust is large enough to oppose buoyancy forces from below, raising the normal stress above lithostatic conditions. Increases in the coefficient of friction could arise from several factors, as μ' contains parameters that model cohesion, pore fluid pressure, and the true coefficient of friction, all of which are poorly constrained. While, the exact mechanism by which mechanical plate coupling could increase is unclear, there is evidence that buoyancy variations influence stress on the interface. Slab buoyancy variations due to thermal age have been linked to earthquake size distributions, with more buoyant (younger) slabs linked to larger earthquakes (Nishikawa and Ide, 2014; Scholz, 2015), which in turn have been linked to fault stress, with larger events corresponding to increased stress (Scholz, 2015; Spada et al., 2013). Assuming that the pattern of current kinematic plate locking reflects the long-term dynamic trends (see Sec. 4.2), observations of increased plate locking above regions of subslab buoyancy (Fig. 4) are consistent with buoyancy-modulated mechanical plate coupling.

Other mantle scale features could potentially influence the megathrust. Particularly the fragmented nature of the slab downdip and the presence of the "slab hole" (Hawley and Allen, 2019; Roth et al., 2008), could impart nonuniform slab pull forces across the margin. How forces due to downdip heterogeneity are distributed up-dip is unknown and it is not clear how they may impact the seismogenic region. Further, variations within the mantle wedge (Gao and Shen, 2014) may impact rheology, fluid fluxes, and flow patterns in the arc and backarc but it is unclear how they may couple into the forearc region. There is still debate on how these features impact the large scale geodynamics of the region (Long, 2016), thus we choose to focus on one aspect of the mantle-megathrust interaction, subslab buoyancy, for which we feel we have good constraints and a compelling mechanism.

4.2. Forearc uplift

We hypothesize that heterogeneity beneath the subducting slab influences where topographic development is most likely to occur within the forearc (Fig. 6). This occurs because subslab buoyancy laterally modulates the long-term total shear force on the interface by shallowing slab dip and/or increasing mechanical plate coupling (see Sec. 4.1). The current state of kinematic plate locking need not reflect long-term dynamic trends; in Cascadia, however, they appear to be consistent over many seismic cycles (Fig. 2, 4; Sec. 3.1), indicating a stable relationship. We observe increased plate locking in the northern and southern segments where we infer an increase in total shear force due to subslab buoyancy. Thus, we suggest that subslab buoyancy influences the pattern of interseismic plate locking for any given seismic cycle.

The distribution and degree of plate locking is a first order control on interseismic deformation (Li et al., 2018; Schmalzle et al., 2014). For Cascadia, the pattern of long-term vertical uplift in the forearc appears to be related to this pattern of interseismic vertical deformation (Fig. 2), however, the values are an order of magnitude lower. This suggests that some fraction of strain is unrecovered during the seismic cycle and is instead converted into permanent deformation (Kelsey et al., 1994). Contributions to the net uplift over the seismic cycle can come from interseismic, coseismic, and postseismic stages (Hu et al., 2016), making it difficult

to parse the relative impact of each phase on long-term deformation. If consistent over many seismic cycles, however, this leads to topographic development. This mechanism has been proposed to explain forearc highs globally (Bassett and Watts, 2015). In this scenario then, subslab buoyancy influences where topography develops by locally increasing the degree of plate locking over many seismic cycles, thus progressively and selectively building up strain unrecovered during the seismic cycle in those regions.

Additional factors may contribute to the kinematics of the Cascadia forearc such as, extension faulting (e.g. along the La Grange fault; Batt et al., 2010; Piotraschke et al., 2015), glacial isostatic adjustments, and variations in sediment supply and accretionary wedge dynamics offshore (Adam et al., 2004; Booth-Rea et al., 2008). Accounting for every constituent of forearc topographic development is beyond the scope of this paper, though some, such as extension, may also be influenced by subslab buoyancy. Instead, we present the above model as a viable argument for subslab buoyancy as a first order contributor to the development of variable forearc topography in Cascadia.

4.3. Support of high forearc topography

Topographic highs in the forearc, once emplaced, must be supported or else gravitational forces in the crustal column will promote relaxation. We have shown that for Cascadia, isostatic forces alone cannot adequately explain the topographic variation (see Sec. 3.2). Instead, we infer that subslab buoyancy alters the slab dip angle and/or mechanical plate coupling along the interface, which locally increases the total shear force that opposes stretching and the collapse of the forearc, thus allowing for higher forearc topography (see Sec. 3.5).

To investigate this, we examine how variations in mechanical plate coupling and slab dip angle could modulate the total supported topography via resistive shear forces. We use the mechanical model from Sec. 3.5 (Eq. (4)) to estimate forearc topography (b) along-strike (as a function of latitude) using observations from the Cascadia margin as guidelines (Fig. 7). This is done not as a precise estimate of topography, but as a conceptual test to verify whether the magnitude and first-order pattern of forearc topography can be explained via our model.

We start by examining the effect of slab dip angle and mechanical plate coupling individually, although we suspect that both properties contribute and may be covariant. First, mechanical plate coupling is held constant (see Sec. 3.5) and slab dip is allowed to vary along-strike with values corresponding to those plotted in Fig. 4b (green line Fig. 7). Next slab dip is held constant ($\beta = 11.5°$) and the mechanical plate coupling is varied. Because we do not know the exact distribution and magnitude of long-term mechanical plate coupling we use the inferred plate locking as a proxy. To do this we multiply the averaged plate locking fraction (Fig. 4c) by a factor of 0.058 and equate it to the μ' term of mechanical plate coupling $\mu'\sigma_n$ (purple line Fig. 7). This is done so that the average plate locking value (54%) is equivalent to the assumed value of $\mu' = 0.03$ from Sec. 3.5.

Allowing both slab dip angle and mechanical plate coupling to vary along-strike we predict higher topography in the northern and southern segments, with local maximums collocated with observed local maximums in forearc topography (black line Fig. 7). Our model successfully predicts the broader spatial pattern of forearc topography in Cascadia and estimates elevations which are generally within ~1 km of the observations. The ability of the model to predict these first-order features suggests that resistive shear forces, modulated along-strike by subslab buoyancy, are a viable mechanism influencing topographic variation in the Cascadia forearc.
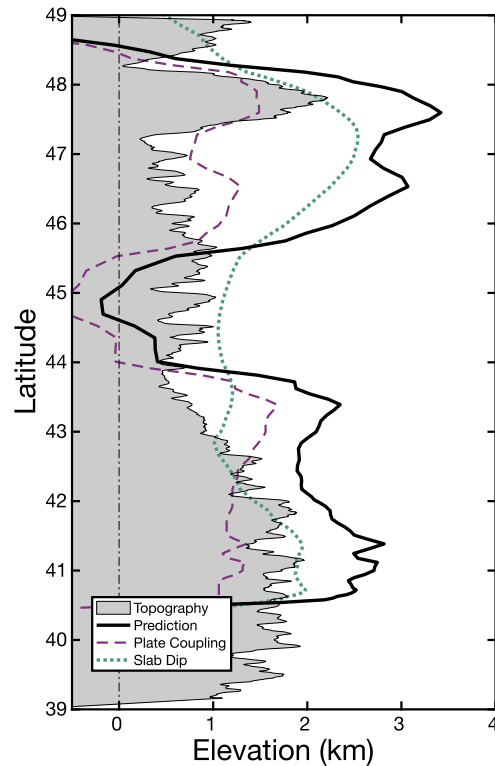

Fig. 7. Predicted topography assuming support comes from the resistive shear force at the megathrust interface. Black line represents the predicted topography using along-strike slab dip angle and plate locking variations as variable inputs. Grey region is the observed maximum topography in the defined swath (Fig. 1). Green line represents the predicted topography only due to variations in slab dip angle. Purple line represents the predicted topography only due to variations in plate locking.

This calculation is presented as a proof of concept rather than a precise estimate as several details are not considered by the model. These include the structure of the forearc (e.g. Delph et al., 2018; Janiszewski et al., 2019), the relationship between long-term mechanical plate coupling and current kinematic plate locking, and precise isostatic contributions from the mantle to the surface, influence from slab structure. These features are also likely important in explaining forearc topography in this region, providing motivation for more detailed modeling in the future. Discrepancies between our model predictions and the observed topography such as the overestimation in the north and south, underestimation in central Cascadia, and differences in the wavelength of topographic features may be due to these unaccounted factors. Finally, our model only considers the 2D influence of subduction related processes, however, 3D processes and edge effects may also be important in Cascadia especially near the Mendocino triple junction region.

5. Conclusion

The topography of the Cascadia forearc is spatially correlated with several independent observations. Regions of high topography in the north and south correspond with increased interseismic uplift rates, increased coseismic subsidence, increased long-term uplift rates, increased erosion rates, low-velocity anomalies in the subslab region, increased inferred subslab buoyancy, shallower slab dip angles, and increased plate locking. We suggest that buoyancy forces arising from subslab heterogeneity modulate the total shear force on the megathrust interface by shallowing the slab dip and/or increasing mechanical plate coupling. In this way, subslab buoyancy can indirectly contribute to subduction processes, influencing where topographic development is most likely to occur and

providing dynamic lateral support for current topographic variations.

Acknowledgements

We would like to thank Editor Miaki Ishii and two anonymous reviewers for their helpful and thoughtful comments on this manuscript. We would also like to thank Emilie Hooft and Roland Bürgmann for their insightful comments on versions of this manuscript. This research was supported by the National Science Foundation under grants OCE-1139701, OCE-1333196, and EAR-1520694 to the University of Oregon.

Appendix A. Supplementary material

Supplementary material related to this article can be found online at https://doi.org/10.1016/j.epsl.2019.115965.

References

Aalto, K.R., 2006. The Klamath peneplain: a review of J.S. Diller's classic erosion surface. Spec. Pap., Geol. Soc. Am. https://doi.org/10.1130/2006.2410(22).

Adam, J., Klaeschen, D., Kukowski, N., Flueh, E., 2004. Upward delamination of Cascadia Basin sediment infill with landward frontal accretion thrusting caused by rapid glacial age material flux. Tectonics. https://doi.org/10.1029/2002TC001475.

Amante, C., Eakins, B.W., 2009. ETOPO1 1 arc-minute global relief model: procedures, data sources and analysis. NOAA Tech. Memo. NESDIS NGDC-24, 1–19. https://doi.org/10.1594/PANGAEA.769615.

Ando, M., 1975. Source mechanisms and tectonic significance of historical earthquakes along the Nankai trough, Japan. Tectonophysics 27 (2), 119–140. https://doi.org/10.1016/0040-1951(75)90102-X.

Balco, G., Finnegan, N., Gendaszek, A., Stone, J.O.H., Thompson, A., 2013. Erosional response to northward-propagating crustal thickening in the coastal ranges of the U.S. pacific northwest. Am. J. Sci. 313 (8), 790–806. https://doi.org/10.2475/11.2013.01.

Bassett, D., Watts, A.B., 2015. Gravity anomalies, crustal structure, and seismicity at subduction zones, 2: interrelationships between fore-arc structure and seismogenic behavior. Geochem. Geophys. Geosyst. 16 (5), 1541–1576. https://doi.org/10.1002/2014GC005685.

Batt, G.E., Cashman, S.M., Garver, J.I., Bigelow, J.J., 2010. Thermotectonic evidence for two-stage extension on the Trinity Detachment Surface, Eastern Klamath Mountains, California. Am. J. Sci. 310 (4), 261–281. https://doi.org/10.2475/04.2010.02.

Bell, S., Ruan, Y., Forsyth, D.W., 2016. Ridge asymmetry and deep aqueous alteration at the trench observed from Rayleigh wave tomography of the Juan de Fuca plate. J. Geophys. Res., Solid Earth 121 (10), 7298–7321. https://doi.org/10.1002/2016JB012990.

Betts, P.G., Mason, W.G., Moresi, L., 2012. The influence of a mantle plume head on the dynamics of a retreating subduction zone. Geology 40 (8), 739–742. https://doi.org/10.1130/G32909.1.

Bierman, P., Clapp, E., Nichols, K., Gillespie, A., Caffee, M.W., 2001. Using cosmogenic nuclide measurements in sediments to understand background rates of erosion and sediment transport. In: Landscape Erosion and Evolution Modeling. Springer US, Boston, MA, pp. 89–115.

Bletery, Q., Thomas, A.M., Rempel, A.W., Karlstrom, L., Sladen, A., De Barros, L., 2016. Mega-earthquakes rupture flat megathrusts. Science 354 (6315), 1027–1031. https://doi.org/10.1126/science.aag0482.

Bodmer, M., Toomey, D.R., Hooft, E.E., Nábelek, J., Braunmiller, J., 2015. Seismic anisotropy beneath the Juan de Fuca plate system: evidence for heterogeneous mantle flow. Geology 43 (12), 1095–1098. https://doi.org/10.1130/G37181.1.

Bodmer, M., Toomey, D.R., Hooft, E.E.E., Schmandt, B., 2018. Buoyant asthenosphere beneath Cascadia influences megathrust segmentation. Geophys. Res. Lett. 45 (14), 6954–6962. https://doi.org/10.1029/2018GL078700.

Booth-Rea, G., Klaeschen, D., Grevemeyer, I., Reston, T., 2008. Heterogeneous deformation in the Cascadia convergent margin and its relation to thermal gradient (Washington, NW, USA). Tectonics. https://doi.org/10.1029/2007TC002209.

Bostock, M.G., Christensen, N.I., Peacock, S.M., 2019. Seismicity in Cascadia. Lithos 332–333, 55–66. https://doi.org/10.1016/j.lithos.2019.02.019.

Brandon, M.T., Calderwood, A.R., 1990. High-pressure metamorphism and uplift of the Olympic subduction complex. Geology 18 (12), 1252–1255. https://doi.org/10.1130/0091-7613(1990)018<1252:HPMAUO>2.3.CO;2.

Brandon, M.T., Roden-Tice, M.K., Carver, J.I., 1998. Late Cenozoic exhumation of the Cascadia accretionary wedge in the Olympic Mountains, northwest Washington State. Bull. Geol. Soc. Am. 110 (8), 985–1009. https://doi.org/10.1130/0016-7606(1998)110<0985:LCEOTC>2.3.CO;2.

Brocher, T.M., 2005. Empirical relations between elastic wavespeeds and density in the Earth's crust. Bull. Seismol. Soc. Am. 95 (6), 2081–2092. https://doi.org/10.1785/0120050077.

Brudzinski, M.R., Allen, R.M., 2007. Segmentation in episodic tremor and slip all along Cascadia. Geology 35 (10), 907. https://doi.org/10.1130/G23740A.1.

Burgette, R.J., Weldon, R.J., Schmidt, D.A., 2009. Interseismic uplift rates for western Oregon and along-strike variation in locking on the Cascadia subduction zone. J. Geophys. Res., Solid Earth 114 (1). https://doi.org/10.1029/2008JB005679.

Byrnes, J.S., Toomey, D.R., Hooft, E.E.E., Nábelek, J., Braunmiller, J., 2017. Mantle dynamics beneath the discrete and diffuse plate boundaries of the Juan de Fuca plate: results from Cascadia Initiative body wave tomography. Geochem. Geophys. Geosyst. 18 (8), 2906–2929. https://doi.org/10.1002/2017GC006980.

Cattin, R., Lyon-Caen, H., Chéry, J., 1997. Quantification of interplate coupling in subduction zones and forearc topography. Geophys. Res. Lett. 24 (13), 1563–1566. https://doi.org/10.1029/97GL01550.

Christensen, N.I., Mooney, W.D., 1995. Seismic velocity structure and composition of the continental crust: a global view. J. Geophys. Res., Solid Earth 100 (B6), 9761–9788. https://doi.org/10.1029/95JB00259.

Cloos, M., 1992. Thrust-type subduction-zone earthquakes and seamount asperities: a physical model for seismic rupture. Geology 20 (7), 601. https://doi.org/10.1130/0091-7613(1992)020<0601:TTSZEA>2.3.CO;2.

Dahlen, F.A., 1990. Fold-and-thrust belts and accretionary wedges. Annu. Rev. Earth Planet. Sci. 18, 55–99. https://doi.org/10.1146/annurev.ea.18.050190.000415.

Delph, J.R., Levander, A., Niu, F., 2018. Fluid controls on the heterogeneous seismic characteristics of the Cascadia margin. Geophys. Res. Lett. 45 (20), 11,021–11,029. https://doi.org/10.1029/2018GL079518.

DeMets, C., Gordon, R.G., Argus, D.F., 2010. Geologically current plate motions. Geophys. J. Int. 181 (1), 1–80. https://doi.org/10.1111/j.1365-246X.2009.04491.x.

Diller, J.S., 1902. Topographic development of the Klamath Mountains. https://doi.org/10.3133/b196.

Eilon, Z.C., Abers, G.A., 2017. High seismic attenuation at a mid-ocean ridge reveals the distribution of deep melt. Sci. Adv. 3, e1602829. https://doi.org/10.1126/sciadv.1602829.

Ferrier, K.L., Kirchner, J.W., Finkel, R.C., 2005. Erosion rates over millennial and decadal timescales at Caspar Creek and Redwood Creek, Northern California Coast Ranges. Earth Surf. Process. Landf. 30 (8), 1025–1038. https://doi.org/10.1002/esp.1260.

Fountain, A.G., Glenn, B., Basagic, H.J., 2017. The geography of glaciers and perennial snowfields in the American West. Arct. Antarct. Alp. Res. 49 (3), 391–410. https://doi.org/10.1657/aaar0017-003.

Fuller, T.K., Perg, L.A., Willenbring, J.K., Lepper, K., 2009. Field evidence for climate-driven changes in sediment supply leading to strath terrace formation. Geology 37 (5), 467–470. https://doi.org/10.1130/G25487A.1.

Gao, H., Shen, Y., 2014. Upper mantle structure of the Cascades from full-wave ambient noise tomography: evidence for 3D mantle upwelling in the back-arc. Earth Planet. Sci. Lett. 390, 222–233. https://doi.org/10.1016/j.epsl.2014.01.012.

Gilbert, H., 2012. Crustal structure and signatures of recent tectonism as influenced by ancient terranes in the western United States. Geosphere 8 (1), 141. https://doi.org/10.1130/GES00720.1.

Goldfinger, C., Nelson, C.H., Morey, A.E., Joel, E.J., Patton, J., Karabanov, E., et al., 2012. Turbidite event history — methods and implications for Holocene paleoseismicity of the Cascadia Subduction Zone. U. S. Geol. Surv. Prof. Pap. 1661.

Hawley, W.B., Allen, R.M., 2019. The fragmented death of the Farallon plate. Geophys. Res. Lett. 2019GL083437. https://doi.org/10.1029/2019GL083437.

Heller, P.L., Ryberg, P.T., 1983. Sedimentary record of subduction of forearc transition in the rotated Eocene basin of western Oregon (USA). Geology. https://doi.org/10.1130/0091-7613(1983)11<380:SROSTF>2.0.CO;2.

Hu, Y., Bürgmann, R., Uchida, N., Banerjee, P., Freymueller, J.T., 2016. Stress-driven relaxation of heterogeneous upper mantle and time-dependent afterslip following the 2011 Tohoku earthquake. J. Geophys. Res., Solid Earth. https://doi.org/10.1002/2015JB012508.

Huybers, P., Langmuir, C.J., 2009. Feedback between deglaciation, volcanism, and atmospheric CO_2. Earth Planet. Sci. Lett. 286 (3–4), 479–491. https://doi.org/10.1016/j.epsl.2009.07.014.

Hyndman, R.D., Wang, K., 1993. Thermal constraints on the Zone of Major Thrust Earthquake Failure' Zone earthquakes that compared the Cascadia subduction across the Cascadia margin the Cascadia margin. J. Geophys. Res. 98 (B2), 2039–2060. https://doi.org/10.1029/95JB01970.

Hyndman, R.D., Wang, K., 1995. The rupture zone of Cascadia great earthquakes from current deformation and the thermal regime. J. Geophys. Res., Solid Earth 100 (B11), 22133–22154. https://doi.org/10.1029/95JB01970.

Janiszewski, H.A., Gaherty, J.B., Abers, G.A., Gao, H., Eilon, Z.C., 2019. Amphibious surface-wave phase-velocity measurements of the Cascadia subduction zone. Geophys. J. Int. https://doi.org/10.1093/gji/ggz051.

Kelsey, H.M., Engebretson, D.C., Mitchell, C.E., Ticknor, R.L., 1994. Topographic form of the Coast Ranges of the Cascadia margin in relation to coastal uplift rates and plate subduction. J. Geophys. Res., Solid Earth. https://doi.org/10.1029/93JB03236.

Kelsey, H.M., Ticknor, R.L., Bockheim, J.G., Mitchell, C.E., 1996. Quaternary upper plate deformation in coastal Oregon. Bull. Geol. Soc. Am. https://doi.org/10.1130/0016-7606(1996)108<0843:QUPDIC>2.3.CO;2.

Kopp, H., 2013. Invited review paper: the control of subduction zone structural complexity and geometry on margin segmentation and seismicity. Tectonophysics 589, 1–16. https://doi.org/10.1016/j.tecto.2012.12.037.

Leonard, L.J., Currie, C.A., Mazzotti, S., Hyndman, R.D., 2010. Rupture area and displacement of past Cascadia great earthquakes from coastal coseismic subsidence. Bull. Geol. Soc. Am. 122 (11–12), 2079–2096. https://doi.org/10.1130/B30108.1.

Li, S., Wang, K., Wang, Y., Jiang, Y., Dosso, S.E., 2018. Geodetically inferred locking state of the Cascadia megathrust based on a viscoelastic Earth model. J. Geophys. Res., Solid Earth 123 (9), 8056–8072. https://doi.org/10.1029/2018JB015620.

Littel, G.F., Thomas, A.M., Baltay, A.S., 2018. Using tectonic tremor to constrain seismic wave attenuation in Cascadia. Geophys. Res. Lett. 45 (18), 9579–9587. https://doi.org/10.1029/2018GL079344.

Livermore, L., 2001. Stochastic processes of soil production and transport: erosion rates, topographic variation and cosmogenic nuclides in the Oregon Coast Range. Earth Surf. Process. Landf. 26, 531–552.

Long, M.D., 2016. The Cascadia paradox: mantle flow and slab fragmentation in the Cascadia subduction system. J. Geodyn. https://doi.org/10.1016/j.jog.2016.09.006.

Marshall, J.A., Roering, J.J., Gavin, D.G., Granger, D.E., 2017. Late quaternary climatic controls on erosion rates and geomorphic processes in western Oregon, USA. Bull. Geol. Soc. Am. 129 (5–6), 715–731. https://doi.org/10.1130/B31509.1.

McCrory, P.A., Blair, J.L., Waldhauser, F., Oppenheimer, D.H., 2012. Juan de Fuca slab geometry and its relation to Wadati-Benioff zone seismicity. J. Geophys. Res., Solid Earth 117 (9), 1–23. https://doi.org/10.1029/2012JB009407.

McNeill, L.C., Goldfinger, C., Kulm, L.V.D., Yeats, R.S., 2000. Tectonics of the Neogene Cascadia forearc basin: investigations of a deformed late Miocene unconformity. Bull. Geol. Soc. Am. 112 (8), 1209–1224. https://doi.org/10.1130/0016-7606(2000)112<1209:TOTNCF>2.0.CO;2.

Mortimer, N., Coleman, R.G., 1985. A Neogene structural dome in the Klamath Mountains, California and Oregon. Geology 13 (4), 253–256. https://doi.org/10.1130/0091-7613(1985)13<253:ANSDIT>2.0.CO;2.

Nishikawa, T., Ide, S., 2014. Earthquake size distribution in subduction zones linked to slab buoyancy. Nat. Geosci. 7 (12), 904–908. https://doi.org/10.1038/ngeo2279.

Parsons, T., Blakely, R.J., Brocher, T.M., Christensen, N.I., Fisher, M.A., Flueh, E., et al., 2005. Crustal structure of the Cascadia Fore Arc of Washington. Earthquake 36. U.S. Geological Survey Professional Paper 1661-D. Retrieved from http://govreports.library.gatech.edu/handle/123456789/599.

Pazzaglia, F.J., Brandon, M.T., 2001. A fluvial record of long-term steady-state uplift and erosion across the Cascadia forearc high, western Washington State. Am. J. Sci. 301 (4–5), 385–431. https://doi.org/10.2475/ajs.301.4-5.385.

Penserini, B.D., Roering, J.J., Streig, A., 2017. A morphologic proxy for debris flow erosion with application to the earthquake deformation cycle, Cascadia Subduction Zone, USA. Geomorphology 282, 150–161. https://doi.org/10.1016/j.geomorph.2017.01.018.

Piotraschke, R., Cashman, S.M., Furlong, K.P., Kamp, P.J.J., Danišík, M., Xu, G., 2015. Unroofing the Klamaths—Blame it on Siletzia? Lithosphere 7 (4), 427–440. https://doi.org/10.1130/L418.1.

Ramírez-Herrera, M.T., Gaidzik, K., Forman, S., Kostoglodov, V., Bürgmann, R., Johnson, C.W., 2018. Relating the long-term and short-term vertical deformation across a transect of the forearc in the central Mexican subduction zone. Geosphere 14 (2), 419–439. https://doi.org/10.1130/GES01446.1.

Riddihough, R., 1984. Recent movements of the Juan de Fuca plate system. J. Geophys. Res., Solid Earth 89 (B8), 6980–6994. https://doi.org/10.1029/JB089iB08p06980.

Roering, J.J., Perron, J.T., Kirchner, J.W., 2007. Functional relationships between denudation and hillslope form and relief. Earth Planet. Sci. Lett. 264 (1–2), 245–258. https://doi.org/10.1016/j.epsl.2007.09.035.

Roering, J.J., Mackey, B.H., Handwerger, A.L., Booth, A.M., Schmidt, D.A., Bennett, G.L., Cerovski-Darriau, C., 2015. Beyond the angle of repose: a review and synthesis of landslide processes in response to rapid uplift, Eel River, Northern California. Geomorphology 236, 109–131. https://doi.org/10.1016/j.geomorph.2015.02.013.

Roth, J.B., Fouch, M.J., James, D.E., Carlson, R.W., 2008. Three-dimensional seismic velocity structure of the northwestern United States. Geophys. Res. Lett. 35 (15), L15304. https://doi.org/10.1029/2008GL034669.

Royden, L.H., Husson, L., 2009. Subduction with variations in slab buoyancy: models and application to the Banda and Apennine systems. In: Subduction Zone Geodynamics, pp. 35–45.

Rychert, C.A., Harmon, N., Tharimena, S., 2018. Scattered wave imaging of the oceanic plate in Cascadia. Sci. Adv. https://doi.org/10.1126/sciadv.aao1908.

Schmalzle, G.M., McCaffrey, R., Creager, K.C., 2014. Central Cascadia subduction zone creep. Geochem. Geophys. Geosyst. 15 (4), 1515–1532. https://doi.org/10.1002/2013GC005172.

Scholz, C.H., 2015. On the stress dependence of the earthquake b-value. Geophys. Res. Lett. 10964. https://doi.org/10.1002/2014GL062863.

Shen, W., Ritzwoller, M.H., Schulte-Pelkum, V., 2013. A 3-D model of the crust and uppermost mantle beneath the Central and Western US by joint inversion of receiver functions and surface wave dispersion. J. Geophys. Res., Solid Earth 118 (1), 262–276. https://doi.org/10.1029/2012JB009602.

Snoke, A.W., Barnes, C.G., 2006. The development of tectonic concepts for the Klamath Mountains province, California and Oregon. Spec. Pap., Geol. Soc. Am. https://doi.org/10.1130/2006.2410(01).

Spada, M., Tormann, T., Wiemer, S., Enescu, B., 2013. Generic dependence of the frequency-size distribution of earthquakes on depth and its relation to the strength profile of the crust. Geophys. Res. Lett. 40 (4), 709–714. https://doi.org/10.1002/2012GL054198.

Tabor, R.W., Cady, W.M., 1978. The structure of the Olympic Mountains, Washington – analysis of a subduction zone. U. S. Geol. Surv. Prof. Pap. 1033.

Trehu, a M., Asudeh, I., Brocher, T.M., Luetgert, J.H., Mooney, W.D., Nabelek, J.L., Nakamura, Y., 1994. Crustal architecture of the Cascadia forearc. Science 266 (5183), 237–243. https://doi.org/10.1126/science.266.5183.237.

Wang, K., 2000. Stress-strain "paradox", plate coupling, and forearc seismicity at the Cascadia and Nankai subduction zones. Tectonophysics 319 (4), 321–338. https://doi.org/10.1016/S0040-1951(99)00301-7.

Wang, Kelin, Dixon, T., 2004. Coupling semantics and science in earthquake research. Eos.

Wang, Kelin, He, J., 1999. Mechanics of low-stress forearcs: Nankai and Cascadia. J. Geophys. Res. 104 (B7), 15191. https://doi.org/10.1029/1999JB900103.

Wang, P.L., Engelhart, S.E., Wang, K., Hawkes, A.D., Horton, B.P., Nelson, A.R., Witter, R.C., 2013. Heterogeneous rupture in the great Cascadia earthquake of 1700 inferred from coastal subsidence estimates. J. Geophys. Res., Solid Earth 118 (5), 2460–2473. https://doi.org/10.1002/jgrb.50101.

Wells, R., Bukry, D., Friedman, R., Pyle, D., Duncan, R., Haeussler, P., Wooden, J., 2014. Geologic history of Siletzia, a large igneous province in the Oregon and Washington Coast Range: correlation to the geomagnetic polarity time scale and implications for a long-lived Yellowstone hotspot. Geosphere 10 (4), 692–719. https://doi.org/10.1130/GES01018.1.

Wells, R.E., Blakely, R.J., Wech, A.G., McCrory, P.A., Michael, A., 2017. Cascadia subduction tremor muted by crustal faults. Geology 45 (6), 515–518. https://doi.org/10.1130/G38835.1.

Willett, S.D., Brandon, M.T., 2002. On steady states in mountain belts. Geology. https://doi.org/10.1130/0091-7613(2002)030<0175:OSSIMB>2.0.CO;2.

Wilson, D.S., 2002. The Juan de Fuca plate and slab: isochron structure and Cenozoic plate motions. Earthquake.